DYNAMIC RESPONSE AND ACOUSTIC FATIGUE* OF STIFFENED COMPOSITE STRUCTURE

J. Soovere

Lockheed-California Company
Burbank, California, USA

1. INTRODUCTION

Aircraft structure made from graphite/epoxy (Gr/E) composites offer a significant weight savings over comparable aluminum alloy structures. The initial application of these composites has been restricted to low load-carrying lightweight structures such as ailerons, flaps, elevators, slats, and fairings to gain in service experience at low risk. The Gr/E composites may also be used in lightly loaded fuselage structures on some vertical/short takeoff and landing (V/STOL) aircraft. For minimum weight, the fuselage structure will be required to operate well into the post-buckling region, with initial buckling just above 1g.

These lightweight structures are very often subjected to a high level jet noise environment, especially during takeoff and landing, which can produce high random vibration stresses in these structures. High cycle fatigue failures, commonly referred to as acoustic fatigue failures, have occurred in these structures [1] , [2] as a result of the random vibration stresses. The V/STOL fuselage can also be subjected, simultaneously, to a thermal environment. Other environmental factors such as moisture penetration, impact damage and lightning strikes may degrade the performance of these structures in a high noise environment.

The compression and shear buckling loads experienced by the fuselage structure introduce peel loads at the skin-stiffener interface similar to those produced by jet noise. Initial studies with Gr/E composites [3] indicated that fasteners provided an improved acoustic fatigue life over structural bonding. For this and other practical reasons, initial application of Gr/E composites to transport aircraft, such as the L-1011 composite aileron [4] , [5] in Figure 1, used mechanical fasteners. Bonding has also been used on some experimental Gr/E acoustic fatigue panels [3] , [6]. Integrally stiffened Gr/E panels [7] , [8] , [9] , [10] , where the skin and stiffeners are cocured, represent the next stage in this development. The peel strength and, therefore, the acoustic fatigue life of these integrally stiffened structures can be further improved by the use of stitching [8] , [11].

This paper summarizes the results obtained from acoustic fatigue and dynamic response tests and the L-1011 composite aileron and integrally stiffened graphite/epoxy panels. The nature of the damping in integrally stiffened composite panels, its theoretical prediction and its implication on internal noise are briefly discussed.

2. COMPOSITE AILERON TEST PROGRAM

The composite aileron was fabricated with a minisandwich skin [4] , [5] in which the Gr/E face sheets were separated by a syntactic (SYNT) core containing glass microballoons. Cocured doublers were located on the inner face sheet at the rib locations. The covers were attached to the Gr/E cloth ribs, and the front and rear spars with fasteners.

*Performed in part under Contracts N62269-80-C-0239, NADC, and NAS 1-15069, NASA, and in part with Lockheed-California Company funding.

The composite aileron test program included the development of random fatigue data by means of double and single cantilever coupons representing the skin-spar and the skin-rib interfaces and the rib bend radius. Typical measured strain distributions [4] are illustrated in Figure 2. The results of these coupon random fatigue data [5] , including the effects from a built-in void adjacent to a fastener head, a single impact damage (0.88 kilogram-meter) adjacent to a fastener head, moisture conditioning and elevated temperature (82°C), are summarized in Figure 3.

In the early design, core compression was experienced along the edges of the doubler [4] , [5] which produced a premature separation of the doubler from the skin along these edges at lower random strain levels (Figure 3). Improvements in the fabrication procedure eliminated this problem [5]. Consequently, the random fatigue data (Figure 3), which involved failures in the outer face sheets adjacent to the countersunk fastener heads, were considered to be more representative of the improved design.

Modal studies conducted on a representative section of the composite aileron, using impedance head hammer tap and loudspeaker excitations, indicated very low damping ratios (Table 1) even after damage [5] from simulated lightning strikes (Figure 4). The damage was mostly confined to the visible surface damage area with very little interlaminar damage. All of the modes dropped in frequency by a small amount, reflecting, in view of the amount of damage sustained, the redundant nature of the composite structure.

The random fatigue data were used, in conjunction with the results of a nonlinearity test, to select the accelerated proof test random spectrum level (Figure 5). Nonlinear panel response (Figure 6) was obtained during the proof test. The measured strains, when compared with the random fatigue data, indicated that the composite aileron would be free of acoustic fatigue failures throughout its design life.

3. COMBINED ACOUSTIC AND SHEAR LOADS

Acoustic fatigue tests were conducted on an integrally J-stiffened Gr/E minisandwich (Figure 7) and a monolithic (Figure 8) panel near initial shear buckling [7] , [10]. Both integrally stiffened panels were designed to an initial shear buckling load of 1786 kilograms per meter (Table 2). The analysis was performed with an anisotropic finite element program (STRAP 5) developed by the Lockheed-California Company. In general, good agreement was obtained between the predicted and measured buckling loads for the three bay monolithic panel and similar four bay monolithic panels tested in another program [12]. The tooling used affected the thickness of the minisandwich panel skin which resulted in a higher measured initial buckling load. Good agreement was obtained between the predicted and measured mode shapes, the latter obtained from Moire fringe patterns measured in the test facility illustrated in Figure 8. The monolithic panel buckled mode shape contained five antinodes in each of the three bays whereas the minisandwich panel exhibited two antinodes only in the large center bay.

The initial buckling was measured with a noncontacting displacement transducer located at an antinode. The initial buckling load was determined from the discontinuity in the load displacement curve [7] , [10] , and from the frequency-load curve (Figure 9). The increase in the damping ratio (Figure 10) in both the critical and noncritical modes, on approaching initial buckling, made it difficult to trace the variation of the modal frequencies through buckling with the impedance head hammer tap method. The higher the critical mode number, the greater the difficulty. This increase in damping on approaching buckling, was previously [13] observed in axial compression tests on stiffened aluminum panels. The damping was also found to be nonlinear in the compression load region. The same result can also be expected for stiffened composite panels under axial compression load.

In spite of the high damping near initial buckling, the overall strain was increased by approximately thirty percent (Figure 11) at the critical location on both panels, when excited with broad band random acoustic loading. Nonlinear response (Figure 12) was obtained in both panels at the higher sound pressure levels.

4. COMBINED ACOUSTIC AND THERMAL ENVIRONMENTS

The effect of a 121°C thermal environment on the sonic fatigue life of integrally stiffened Gr/E panels, representative of potential fuselage structure, was investigated [7] , [9] using two advanced J-stiffened monolithic panels and two advanced blade stiffened orthogrid panels, illustrated in Figures 13 and 14, respectively. These panels were also designed to an initial shear buckling load of 1786 kilograms per meter (Table 2). The panels were mounted, in turn, into a steel test frame in which the thermal expansion was matched biaxially to that of the composite panel. In the modal studies, heat was applied to the outer surface of the panels by six infrared lamps and the excitation was provided by impedance head hammer taps at preselected grid points. The excitation and the corresponding displacement were analyzed within the Hewlett-Packard HP 5451C Fourier Analyzer to obtain the resonant frequencies, damping ratios and mode shapes.

The measured fundamental mode shape for both panels is illustrated in Figure 15. The fall-off in the resonant frequencies with temperature (Figure 16), observed for both panel configurations, is due to thermally induced bi-axial compression loads in the skin, introduced by differences in the thermal expansion of the Gr/E frames and skin because of differences in their fiber orientations. The temperature does not appear to have affected the damping in both the monolithic and the orthogrid panels (Table 3). The fundamental mode damping ratio in the orthogrid panel is, however, an order of magnitude greater than that in the monolithic panel. The damping in the higher order panel modes is more comparable and very low for both panels.

One panel of each design was acoustic fatigue tested at ambient temperature and the other at a temperature of 123°C. Heat was supplied by a specially designed quartz lamp heater panel, mounted inside the progressive wave tunnel. An overall sound pressure level of 167 dB (Table 4) was used to fail the room temperature orthogrid panel (Figure 14). In contrast, the room temperature and elevated temperature monolithic panels were failed with an overall sound pressure level between 160.8 to 164 dB. The difference in the sound pressure level required to produce the same long side rms strain (Table 4) in the orthogrid and monolithic ambient temperature panels can be attributed to the effect expected from the differences in their fundamental mode damping, even in the presence of nonlinear panel response (Figure 17). The failure obtained with the orthogrid panel does not reflect the true capability of the design since these panels contained stress concentrations at the ends of the longitudinal stiffeners (Figure 14) where the failure was initiated.

In spite of some indications that the temperature of 123°C could affect the sonic fatigue life, the results are considered inconclusive on account of the small sample size. The current room temperature semi-empirical analysis method [6] did not predict the rms strains in the room temperature panels with any degree of accuracy (Table 4). The main reason is thought to be the omission of damping in the above method although differences in the spectrum shape of the random noise may also be a contributing factor.

5. RANDOM FATIGUE DATA FOR INTEGRALLY STIFFENED Gr/E PANELS

Random fatigue data were developed with double cantilever coupons (Figure 18), representing the skin-longitudinal stiffener interface, for the integrally stiffened monolithic (Figure 19) and orthogrid (Figure 20) panels at room temperature. The monolithic coupon data exhibited higher rms strain (Figure 19) levels than the bonded panel data in reference [6]. The monolithic panels could withstand even higher strains than the corresponding coupons. Stitching (Figure 18), also illustrated in cross-section in (Figure 21), increased the failure strain level by approximately 70 percent, comparable to the improvement measured in static peel tests [11].

The orthogrid coupons (Figure 20) achieved an rms strain level comparable to that measured in the composite aileron skin at a KT of 1, and that achieved with stitching in the monolithic coupon. The composite aileron and the orthogrid panel had the same fiber orientation in the face sheets. The orthogrid panel failed well below the coupon strain level indicating the magnitude of the stress concentration at the ends of the axial stiffeners.

6. THEORETICALLY PREDICTED DAMPING FOR THE ORTHOGRID PANELS

Fastener related damping has been eliminated in integrally stiffened composite panels while the material damping is very small, usually below a viscous damping ratio of 0.001 for Gr/E composites. Consequently the only source of significant damping is acoustic radiation, once the energy loss to the surrounding structure has been minimized. A characteristic of acoustic radiation is that the damping is high in the fundamental mode and falls off with increase in mode number due to the cancellation effect [14]. Furthermore, the acoustic radiation is proportional to panel area and should be very large in the fundamental mode of a large single panel. These conditions have been met by the damping ratios in Table 3. The predominant contribution of acoustic radiation to the damping has also been confirmed with stiffened composite honeycomb panels [15]. The orthogrid panel represents an ideal example for demonstrating the above conclusion. The simplified expression in reference [14], for the viscous damping ratio produced by acoustic radiation from a simply supported panel, was used. The measured and predicted damping ratio in Figure 22 are in reasonable agreement, particularly for the fundamental mode, when considering the simplicity of the analysis.

7. CONCLUSIONS

The importance of developing nonlinear analysis capability for design purposes has been demonstrated since composite structures can sustain high vibration levels, in the nonlinear response region, over a wide range of combined loads and environmental conditions without failure. All of the random fatigue data exhibited a fatigue limit just beyond 10^7 cycles, an important consideration for the design of acoustic fatigue resistent composite structures. The acoustic fatigue resistance in integrally stiffened composite structures can be considerably improved by attention to detailed design at the critical locations. In this respect, the integrally stiffened panels are considered to be superior to secondary bonded panels. Since the damping in integrally stiffened composite panels is due to acoustic radiation, the transmission of turbulent boundary layer noise, through the lighter weight integrally stiffened composite fuselage structure, could be significantly increased, over current fuselage structure, for the same density of acoustic sidewall treatment. A compensating increase in the sidewall treatment density could eliminate much of the weight-saving achieved with composite fuselage structure.

REFERENCES

1. T.R. RIEBEN 1957 WADC-TR-57-513. Sonic Fatigue Testing and Development of Aircraft Panels.

2. E.J. RICHARDS 1960 WADC-TR-59-676. An Introduction to Acoustic Fatigue.

3. M.J. JACOBSON 1972 AFFDL-TR-71-126. Advanced Composite Joints; Design and Acoustic Fatigue Characteristics.

4. J. SOOVERE 1980 The Shock and Vibration Bulletin, No. 50, Part 4. Sonic Fatigue Testing of NASA L-1011 Composite Aileron.

5. J. SOOVERE 1982 Journal of Aircraft, 19, No. 4. Sonic Fatigue Testing of an Advanced Composite Aileron.

6. I. HOLEHOUSE 1980 AFWAL-TR-80-3019. Sonic Fatigue Design Techniques for Advanced Composite Aircraft Structures.

7. J. SOOVERE 1982 NADC-78169-60. Effect of Acoustic, Thermal and Shear Loading on Flat Integrally Stiffened Graphite/Epoxy Fuselage Panels.

8. M.J. JACOBSON 1981 NADC-81045-60. Fatigue of V/STOL Composite Fuselage Panels Under Acoustic-Thermal Environments.

9. J. SOOVERE 1983 24th Structures, Structural Dynamics and Materials Conference, Lake Tahoe, Nevada, USA. The Effect of Acoustic-Thermal Environments on Advanced Composite Fuselage Panels.

10. J. SOOVERE 1983 Second United States/Japan Conference on Composite Materials NASA-Langley Research Center, Hampton, Virginia, USA. Dynamic Response of Flat Integrally Stiffened Graphite/Epoxy Panels Under Combined Acoustic and Shear Loads.

11. J. SOOVERE 1980 LR 29410; 1982 LR 30126; Lockheed Reports. Acoustic Response of Composite Panels Under Combined Loading - Parts 1 and 2.

12. R.B. OSTROM 1981 NADC-78137-60. Post-Buckling Fatigue Behavior of Flat, Stiffened Graphite/Epoxy Panels Under Shear Loading.

13. J. SOOVERE and S.T. CHIU 1976 AFFDL-TR-76-65. Effects of Combined Acoustic and Flight Loads on Crack Growth.

14. D.J. MEAD 1964 AFML-TR-65-284. The Effect of Certain Damping Treatments on the Response of Idealized Aeroplane Structures Excited by Noise.

15. J. SOOVERE Ph.D. Thesis, University of Southampton. Dynamic Response of Acoustically Excited Stiffened Composite Honeycomb Panels (In Preparation).

TABLE 1. MODAL FREQUENCIES AND DAMPINGS

UNDAMAGED AILERON		AFTER SIMULATED LIGHTNING STRIKES	
FREQUENCY, Hz	VISCOUS DAMPING RATIO	FREQUENCY, Hz	VISCOUS DAMPING RATIO
96.4	0.0042	91.18	0.0063
125.9	...	109.2	0.0038
134.3	0.0040	119.2	0.0067
149.0	0.010	126.6	0.0065
...	...	129.7	0.0091

TABLE 2. INITIAL SHEAR BUCKLING LOAD

TYPE OF PANEL	LENGTH mm	WIDTH mm	THICKNESS mm	SKIN LAYUP	N_{XYCR} Kg/M	
					STRAP 5	TEST AVERAGE
J-Stiffened Monolithic	546	152	0.89	$(\pm 45/0/\overline{90})_s$	1821*	1759**
	533	180	1.02	$(45/0/-45/90)_s$	1893*	1789 - 1841
J-Stiffened Minisandwich	533	304	1.52	$(45/0/-45/SYNT)_s$	1839*	2419 - 2682
Advanced J-Stiffened Monolithic	737	180	1.02	$(45/0/-45/90)_s$	1839*	--
Advanced Orthogrid	660	254	1.40	$(45/0/-45/SYNT)_s$	1839*	--

* Target Value 1786 Kg/M
** Reference [12]

Subscript s means symmetrically laminated.

TABLE 3. MONOLITHIC AND ORTHOGRID PANEL RESONANT FREQUENCIES AND VISCOUS DAMPING RATIOS

MODE NUMBER	MONOLITHIC PANEL						ORTHOGRID PANEL					
	J2				J1		01				02	
	AMBIENT TEMPERATURE		123 DEGREES CENTIGRADE TEMPERATURE		AMBIENT TEMPERATURE		AMBIENT TEMPERATURE		123 DEGREES CENTIGRADE TEMPERATURE		AMBIENT TEMPERATURE	
	FREQUENCY Hz	DAMPING RATIO	FREQUENCY Hz	DAMPING RATIO	FREQUENCY Hz	DAMPING RATIO	FREQUENCY Hz	DAMPING RATIO	FREQUENCY Hz	DAMPING RATIO	FREQUENCY Hz	DAMPING RATIO
1,1	178.9	0.0058	154.1	0.0046	160.52	0.0043	171.3	0.0473	159.3	0.0402	178.3	0.0393
2,1	262.9	0.0020	225	0.0036	243.1	0.0026	273.2	0.0226	242.5	0.0079	273.4	0.02354
3,1	324.25	0.0025	281.9	0.0042	303.9	0.0030	370.9	0.0015	293.7	0.0132	373.4	0.0028
4,1 Center Bay	389.0	0.0009	341.8	0.0032	359.7	0.0026	460.8	0.0043	394.7	0.0034	457.5	0.0064
4,1 All Bays In Phase	434.4	0.0044	388.7	0.0028	397.8	0.0089	--	--	--	--	--	--
All Bays Out-Of-Phase	--	--	461.1	0.0012	487.1	0.0040	--	--	--	--	--	--

TABLE 4. SUMMARY OF SONIC FATIGUE REST RESULTS AND ANALYTICAL PREDICTIONS

PANEL NUMBER	TEST RESULTS						ANALYSIS [6]			
	OVERALL NOISE LEVEL AT PANEL LOCATION dB	NOISE SPECTRUM LEVEL AT PANEL LOCATION dB/Hz	MAXIMUM RMS STRAIN μ mm/mm		TEST TIME HOURS/ MINUTES	NUMBER OF CYCLES	LONG SIDE RMS STRAIN μ mm/mm	FIXED FIRST MODE FREQ. Hz	NUMBER OF HOURS/ MINUTES	NUMBER OF CYCLES
			LONG SIDE	SHORT SIDE						
J1	157.4	130.9	717	680	5/0*	7.2×10^6	--	--	--	--
	161.0	134.5	900	850	5/0*	7.2×10^6	503	200	6/25	3.9×10^6
	163.4	136.9	1300	1250	0/10**	2×10^5	663	200	0/43	5.2×10^5
J2***	158.4	131.3	460	581	5/0*	5×10^6	--	--	--	--
	160.8	134.3	573	704	3/14**	3.2×10^6	492	200	6/15	4.5×10^6
02	167.0	140.5	490	830	2/20**	2.94×10^6	998	151	0/24	$<2 \times 10^5$****
01***	167.0	140.5	566	745	4/39*	5.86×10^6	998	151	0/24	$<2 \times 10^5$****

*No Failure
**Panel Failed in Sonic Fatigue
***123°C Temperature
****No Test Data in Reference [6] Below 2×10^5

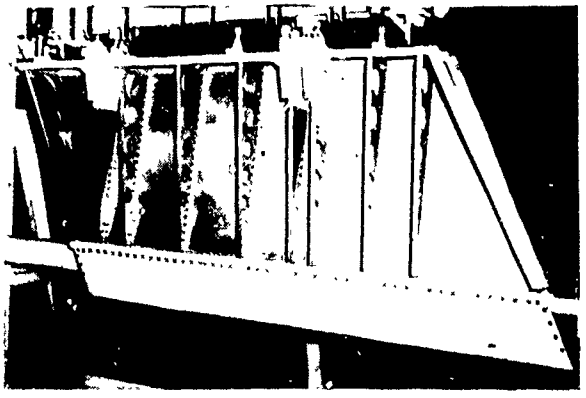

Figure 1. L-1011 Composite Inboard Aileron with the Lower Cover Removed

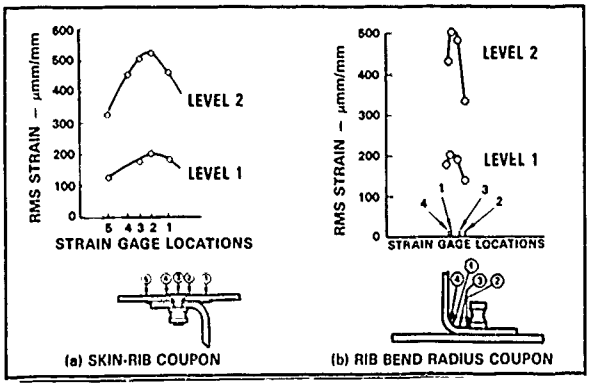

Figure 2. Typical Measured Strain Distribution

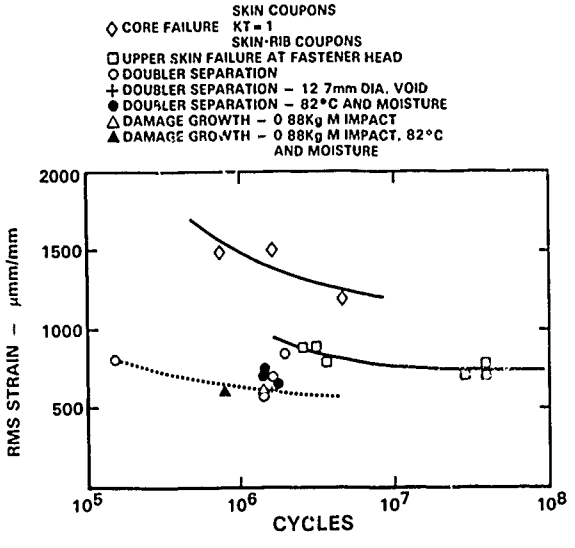

Figure 3. Random Fatigue Data for the Skin and the Skin/Stiffener Interface

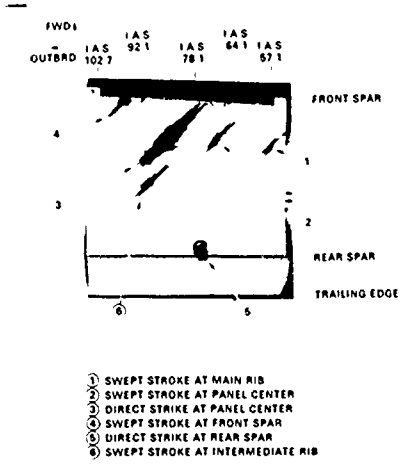

Figure 4. Exterior of Composite Aileron After Lightning Strike Tests

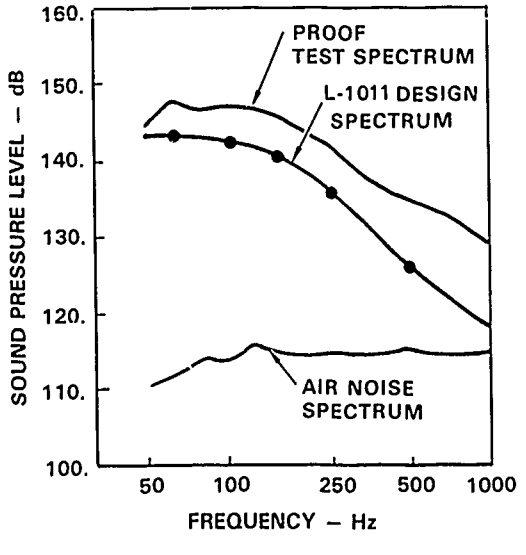

Figure 5. Inboard Aileron Design, Proof Test, and Air Noise 1/3-Octave Band Spectra

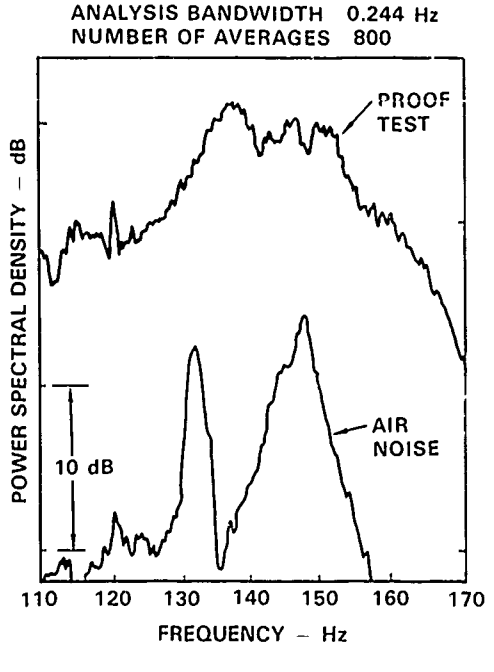

Figure 6. Narrow-Band Analysis of Aileron Strain Data

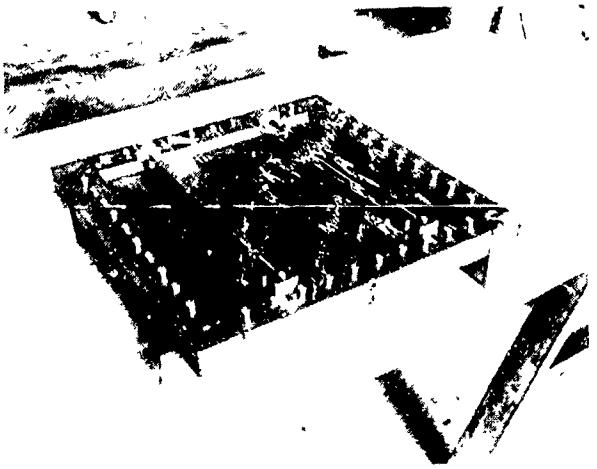

Figure 7. Reverse Side of Shear Frame Showing Stiffener Pivot Attachments - J-Stiffened Minisandwich Panel

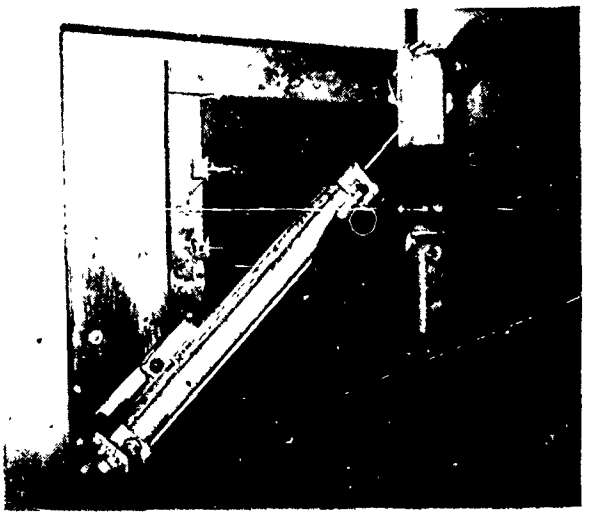

Figure 8. Load Frame in Acoustic Progressive Wave Tunnel Wall Configured for Shear Load - J-Stiffened Monolithic Panel

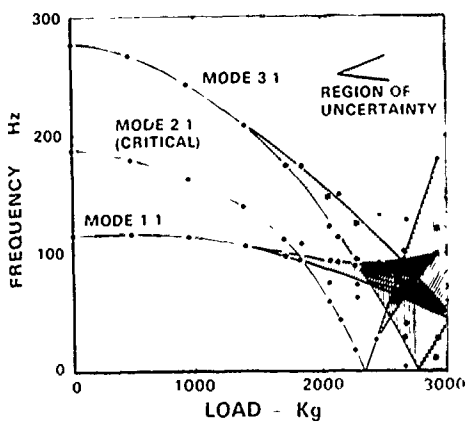

Figure 9. J-Stiffened Minisandwich Panel Frequency Variation as a Function of Jack Load

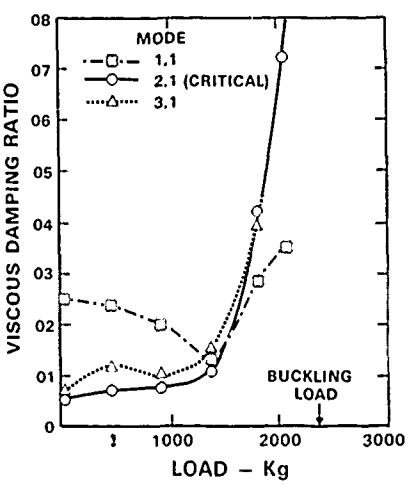

Figure 10. Variation of Damping with Jack Load for J-Stiffened Minisandwich Panel

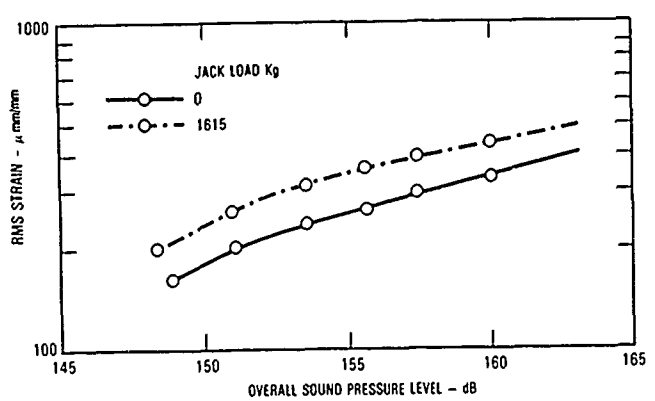

Figure 11. Variation of Overall Sound Pressure Level - J-Stiffened Monolithic Panel

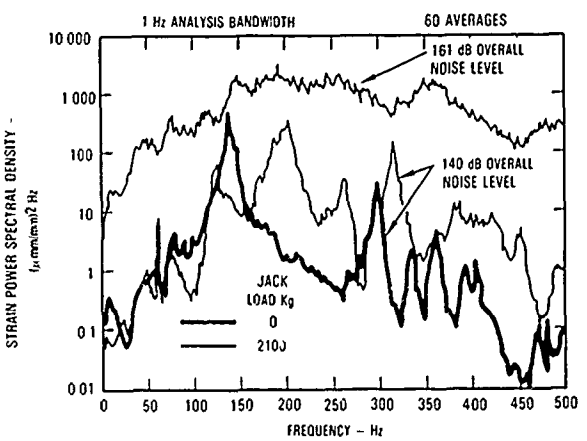

Figure 12. Strain Power Spectral Density for J-Stiffened Minisandwich Panel

Figure 13. J-Stiffened Monolithic Graphite/Epoxy Panel

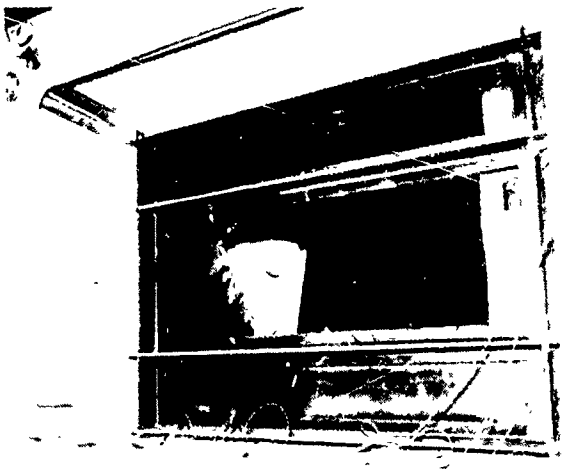

Figure 14. Acoustic Failure in Blade Stiffened Orthogrid Graphite/Epoxy Panel

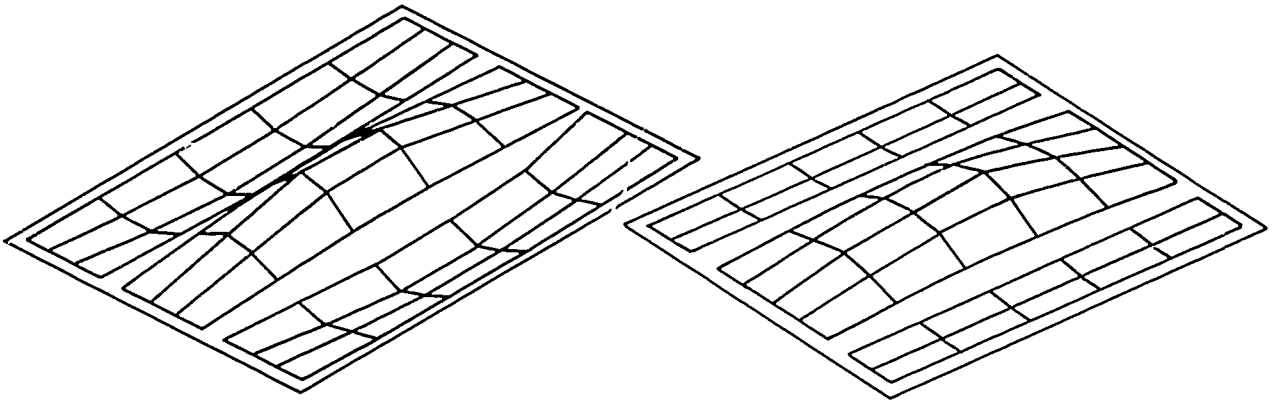

(a) Monolithic Panel

(b) Orthogrid Panel

Figure 15. Measured Panel Fundamental Mode Shape

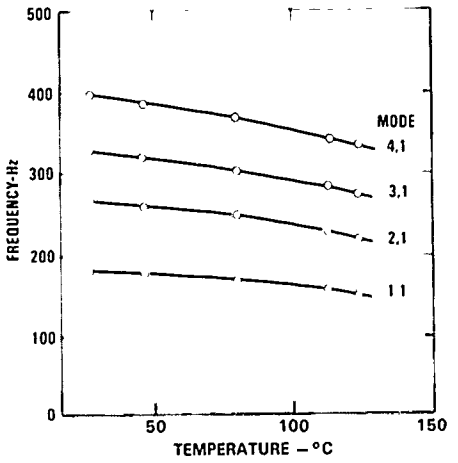

Figure 16. Variation of Modal Frequencies with Temperature - Monolithic Panel

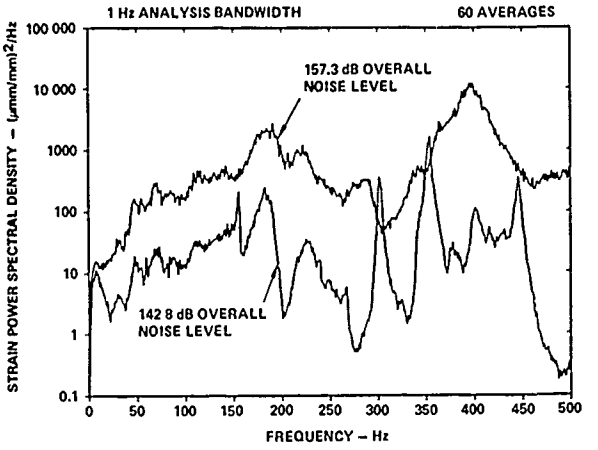

Figure 17. Typical Strain Power Spectral Densities for Monolithic Panel

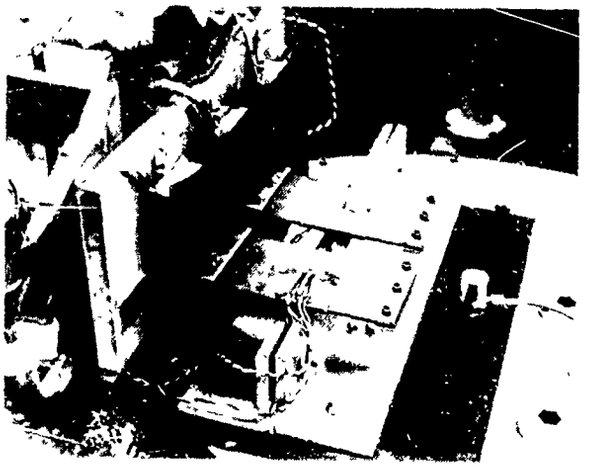

Figure 18. Unstitched and Stitched Coupons Mounted on Electromagnetic Shaker

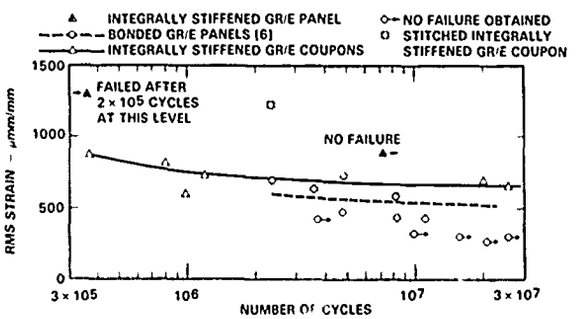

Figure 19. Ambient Temperature Random Fatigue Data from Monolithic Panels and Coupons

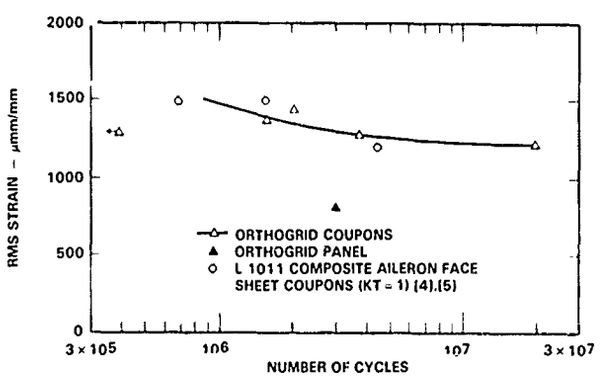

Figure 20. Ambient Temperature Random Fatigue Data from Orthogrid Coupons and Panel

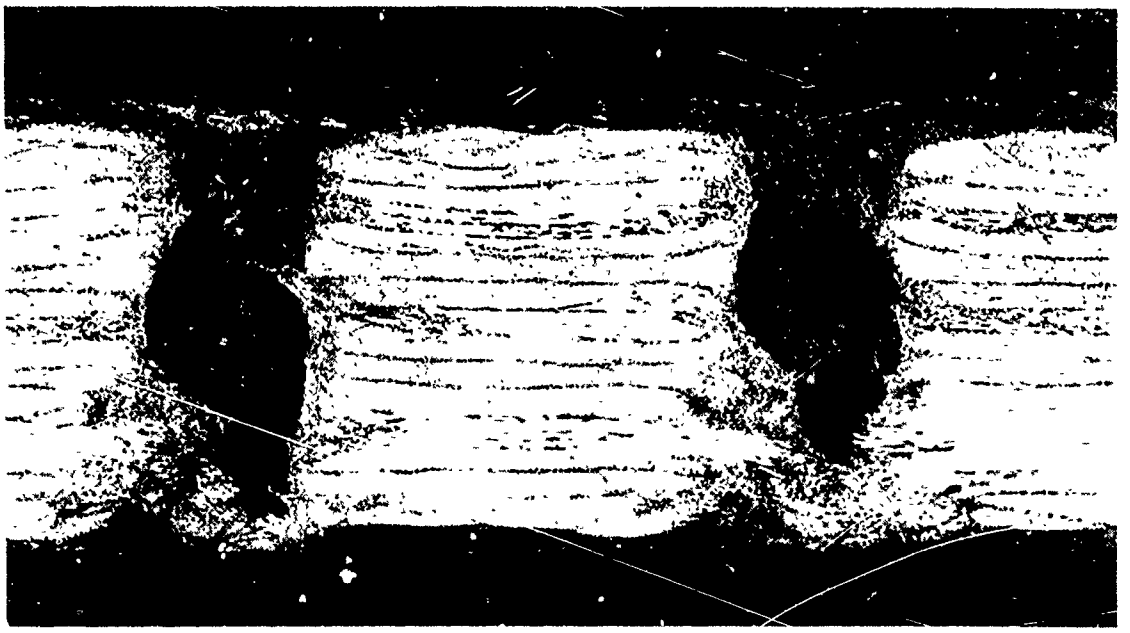

Figure 21. Sectional Micrograph Through Stiffener Flange and Panel Along the Stitch Line - X25 Magnification

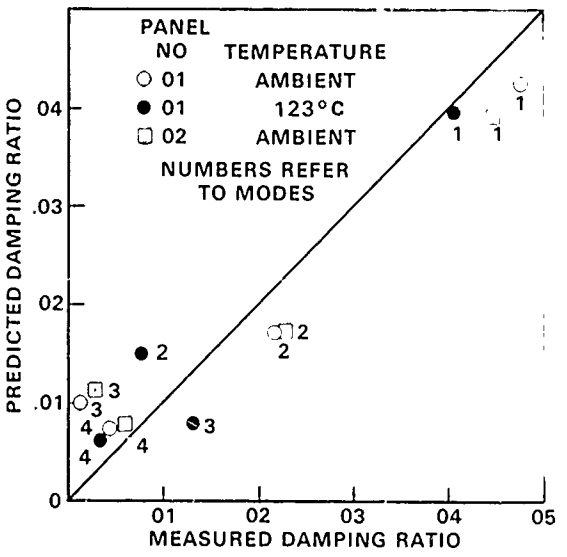

Figure 22. Comparison of Predicted and Measured Orthogrid Panel Damping